ISSN 1674-1056
http://cpb.iphy.ac.cn
http://iopscience.iop.org/cpb
中国物理 B
Chinese Physics
中国物理
Chinese Physics B

Quantum density functional theory investigation to prevail structural, elastic, and opto-electronic attributes of $ZMoO_3$ (Z=Ba and Sr) under pressure

Saad Tariq, A A Mubarak, Saher Saad, M Imran Jamil, S M Sohail Gilani

Citation: Chin. Phys. B . 2019, 28(6): 066101. **doi:** 10.1088/1674-1056/28/6/066101
Journal homepage: http://cpb.iphy.ac.cn; http://iopscience.iop.org/cpb

What follows is a list of articles you may be interested in

Effects of Al component content on optoelectronic properties of $Al_xGa_{1-x}N$

Yan-Jun Ji(纪延俊), Jun-Ping Wang(王俊平), You-Wen Liu(刘友文)

Chin. Phys. B . 2018, 27(10): 106102. **doi:** 10.1088/1674-1056/27/10/106102

Bandgap engineering to tune the optical properties of $Be_xMg_{1-x}X$ (X=S, Se, Te) alloys

B Sabir, N A Noor, M Rashid, Fasih Ud Din, Shahid M Ramay, Asif Mahmood

Chin. Phys. B . 2018, 27(1): 016101. **doi:** 10.1088/1674-1056/27/1/016101

Ab-initio investigation of $AGeO_3$ (A=Ca, Sr) compounds via Tran–Blaha-modified Becke–Johnson exchange potential

Rasul Bakhsh Behram, M A Iqbal, Muhammad Rashid, M Atif Sattar, Asif Mahmood, Shahid M Ramay

Chin. Phys. B . 2017, 26(11): 116103. **doi:** 10.1088/1674-1056/26/11/116103

Electronic, optical, and mechanical properties of BN, AlN, and InN with zinc-blende structure under pressure

A R Degheidy, E B Elkenany

Chin. Phys. B . 2017, 26(8): 086103. **doi:** 10.1088/1674-1056/26/8/086103

Large scale silver nanowires network fabricated by MeV hydrogen (H^+) ion beam irradiation

Honey S, Naseem S, Ishaq A, Maaza M, Bhatti M T, Wan D

Chin. Phys. B . 2016, 25(4): 046105. **doi:** 10.1088/1674-1056/25/4/046105

Quantum density functional theory studies of structural, elastic, and opto-electronic properties of $ZMoO_3$ (Z =Ba and Sr) under pressure

Saad Tariq[1,5,†], A A Mubarak[2], Saher Saad[3], M Imran Jamil[4], and S M Sohail Gilani[3,5]

[1] *Center of Excellence in Solid State Physics, University of Punjab, Lahore* 54590, *Pakistan*
[2] *Physics Department, Rabigh College of Science and Arts, King Abdulaziz University, Jeddah, Saudi Arabia*
[3] *Center for High Energy Physics, University of the Punjab, Lahore* 54590, *Pakistan*
[4] *Department of Physics, School of Science, University of Management and Technology, Lahore* 54770, *Pakistan*
[5] *Faculty of Science, University of Central Punjab, Campus* 2*C, Lahore* 54000, *Pakistan*

(Received 10 December 2018; revised manuscript received 4 March 2019; published online 29 May 2019)

In continuation of our recent report on molybdates [*Appl. Phys. A* **124**, 44 (2018)], the structural, electronic, elastic, and optical properties of $ZMoO_3$ (Z =Ba and Sr) molybdates are investigated under pressure (10 GPa–50 GPa) comprehensively by deploying the density functional theory. Our investigations show that the studied compounds exhibit stable cubic phase with metallic attributes. The thermodynamic parameters such as enthalpy of formation, Debye, and melting temperatures of the compounds are observed to increase with pressure. While the Grüninsen parameter and the coefficient of super-plastic deformation decrease as the pressure increases. Mechanical properties elucidate an increase in measured values of hardness, bulk, shear, and young's moduli with pressure. Our results suggest that the studied compounds are useful in high pressure optoelectronic devices. The optical properties of $BaMoO_3$ (BMO) and $SrMoO_3$ (SMO) are computed for the radiation of up to 35 eV. The present compounds show beneficial optical applications in the anti-reflection coating, lenses, and the high avoiding solar heating applications in the variant applied pressure.

Keywords: optical properties, high pressure, elastic properties, electronic properties

PACS: 61.50.–f, 62.20.D–, 74.62.Fj, 31.15.E– **DOI:** 10.1088/1674-1056/28/6/066101

1. Introduction

Computational techniques such as density functional theory are becoming very popular with time for scrutinizing chemical and physical attributes of solids.[1–7] One can solve and understand complex quantum mechanical, many body, and problems with ease of computation before proceeding towards experimentation.[8–15] Furthermore perovskite compounds have gained noticeable attention due to their extensive usage in electronic devices such as infrared sensors, modulators, memory storage devices, detectors, capacitors for high-frequency microwave devices, photonic crystals and in the nuclear magnetic resonance imaging.[16–22] Molybdenum based compounds also have topological semi-metallic nature with applications in the magneto-electric effects.[23]

Recently, research interest in solid state physics has grown for the exploration of novel emergent phenomena under high pressure conditions. Pressure can reduce the interatomic distances effectively and thus strengthen the electron transfer by enlarging the orbital overlap integral in the strongly correlated electron systems. In particular, material properties will undergo alterations which in result develop a wide range of new compounds. Thus, pressure is a very useful tool for the synthesis of new materials.[24] The application of high pressure would allow one to disentangle the physical properties of interest from the ambient one. It can give not only a critical check on some of the theoretical proposals but provides important implications for the practical applications as well. With the advances of high pressure techniques, researchers have thus focused more on physical properties under extreme conditions.[25] In our very recent study,[26] we have used the same quantum mechanical technique, *i.e.*, density functional theory, to understand the behavior of $BaMoO_3$ and $SrMoO_3$perovskite compounds at the ambient conditions. Here, we are continuing our recent work on $BaMoO_3$ (BMO) and $SrMoO_3$ (SMO) cubic oxides and going to the 50-GPa range.

In neutron diffraction study, performed by Nasif *et al.*,[27] $ZMoO_3$ (Z =Ba and Sr) have been classified as superconducting materials. While, Mizoguchi *et al.*[28] pored over the electronic structure of $ZMoO_3$ (ZMO) experimentally and found a high conductivity of both of the compounds. In another work, Mizoguchi *et al.*[29] studied optical properties and found SMO as an optically transparent material around plasma frequency, whereas thermoelectric properties of BMO have been reported[30] as the compound has extremely high thermal conductivity. In another study, catalytic properties of

†Corresponding author. E-mail: saadigi@hotmail.com
© 2019 Chinese Physical Society and IOP Publishing Ltd

ZMO have been reported by Kubo *et al.*[31] While, in a report by Wang *et al.*, SMO exhibits high metallic conductance[32] and shows transparency in ultraviolet region.[32] These aforementioned studies suggest for the application of SMO as a transparent conducting electrode. Therefore, SMO was proposed[33] to be suitable for microwave devices. Most recently, $Ba_{1-x}Sr_xMoO_3$ solid solutions have been studied by Sahu *et al.*[34] They found that the specific heat of the compound increased as the concentration increased. Later on in 2016, optical properties of $Sr_{1-x}Ba_xMoO_3$ solid solutions were investigated as well by Hopper *et al.*[35] Because both the compounds were prepared by reduction process and exhibited metallic behavior, they are extensively potentially useful for photo catalytic applications.[27,36,37]

In the past, all the above mentioned discussions on ZMO's were primarily on the structural synthesis along with the origin of metallic conductivity. We have found in the literature that there are no reports on thermal, elastic, and optoelectronic traits of ZMO's under pressure. Therefore, in this article, our main focus is to elaborate the hidden attributes of ZMO's under hydrostatic pressure.

2. Computational formalism

Our calculations are implemented by the density functional theory and linearized augmented plane wave method (LAPW),[38–40] which is embodied within state of the art WIEN2k code.[41] Quantum mechanics of the strongly correlated system has been solved using exchange correlation potentials and suggested by generalized gradient approximations (GGA).[42] We have used the values 2.50 a.u., 1.89 a.u., and 1.72 a.u. (the unit a.u. stands for atomic units) as Muffin–Tin radii R_{MT} for $Z =$ (Ba and Sr), Mo, and O respectively. To obtain the full convergence of self-consistent field in the entire Brillouin zone, the denser k-mesh of 2000 k-points was used. The orbital angular momentum l_{max} value was set at 12 for the full wave function expansion. To obtain elastic properties, single unit cell optimizations were performed under small strains along tetrahedral and rhombohedral directions.

3. Results and discussions

3.1. Structural optimizations under pressure

The cubic oxide-perovskite $ZMoO_3$ ($Z =$ Ba and Sr) compounds, with a space group of Pm-3m, hold one molecule in the unit cell structure. The atomic Wyckoff positions of the content atoms are at (0, 0, 0)1a, (0.5, 0.5, 0.5)1b, and (0.5, 0.5, 0)3c for Z, Mo, and three oxygen atoms, respectively. The energy optimizations in Fig. 1 are used to suggest the ground state of the lattice constants for the stable crystalline structures.

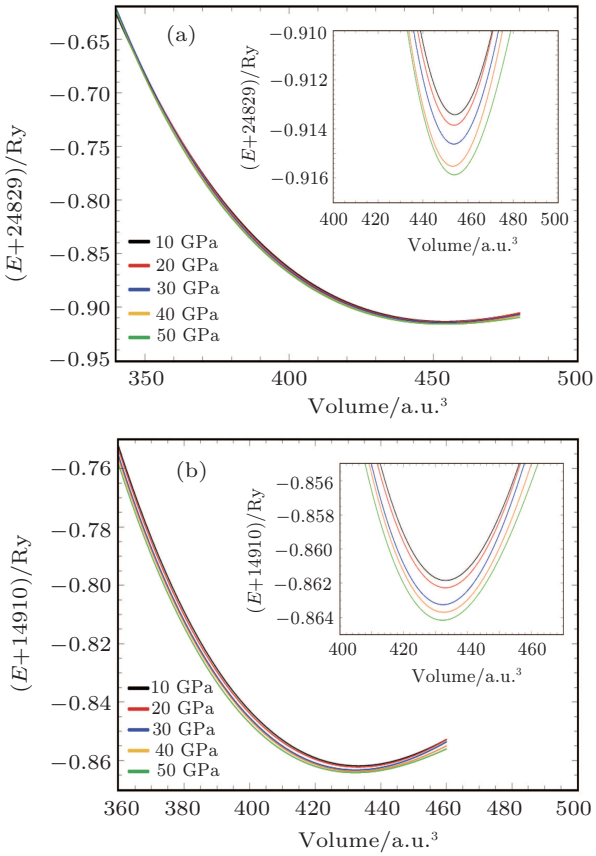


Fig. 1. The structural optimization under different pressures: (a) BMO and (b) SMO.

In the first step, optimized lattice constants of the cubic oxide-perovskite $BaMoO_3$ and $SrMoO_3$ are calculated at 0 GPa with values 4.039 Å and 3.999Å, respectively, which are reported in the previous literature.[26] The obtained data at 0 GPa was then used in the equation[43]

$$P = \frac{B}{B'}\left[\left(\frac{V_0}{V}\right)^{B'} - 1\right]$$

to obtain cubic lattice constants under pressure variations. These lattice constants were used further to obtain optimizations, computed using the Murnaghan equation of states,[44] under pressure variations. These lattice constants a and ground state energies E are listed in Table 1. The variations in optimized ground state energies with increase in pressure can also be observed in Table 1. It has been found that as the pressure increases, the ground state energy decreases. Lowest ground state energy has been found at 50-GPa pressure, so compounds retain their stable cubic phase under pressure. This is because the induced pressure contracts the interatomic distances ($r_A + r_O$ and $r_B + r_O$) that also decreases the bonding distances between ions in the unit cell, as presented in Table 1. The calculated enthalpy of formation energies ΔH_f under variant pressures are listed in Table 1 as well. These values are computed by subtracting the energy of the content atoms of

the compound from the total energy of the compound, *i.e.*,

$$\Delta H_{\rm f} = E_{\rm ZMoO_3} - (E_Z + E_{\rm Mo} + 3E_{\rm O}).$$

The energy of constituent atoms has been obtained by computing the ground state energies of Mo and Sr atoms in *Fm3m* phase, Ba in *Im*-3*m* phase, and O in *C*2/*m* phase. The negative sign of the calculated $\Delta H_{\rm f}$ values indicates that the studied compounds are thermodynamically stable under induced pressure.

The structural stability of BMO and SMO under induced pressure can be checked by Goldschmidt's tolerance factor, $t = (r_{\rm A} + r_{\rm O})/\sqrt{2}(r_{\rm B} + r_{\rm O})$,[45] where $r_{\rm A} + r_{\rm O}$ and $r_{\rm B} + r_{\rm O}$ represent the inter atomic distances between Ba–O (Sr–O), and Mo–O, respectively. The compound is assumed to be stable when $t$lies in between 0.94–1.05 for the cubic perovskite compounds. For the present compounds the value of t lies in the same range (see Table 1). The tolerance values in Table 1 approve the reliability of the performed calculations.

Table 1. Pressure P, lattice constant a, total energy of the bulk system E, enthalpy of formation $\Delta H_{\rm f}$, interatomic distances between content atoms ($r_{\rm A} + r_{\rm O}$ and $r_{\rm B} + r_{\rm O}$), and tolerance factor t.

Compound	P/GPa	a/Å	E/Ry	$\Delta H_{\rm f}$eV	$r_{\rm A} + r_{\rm O}$/a.u.	$r_{\rm B} + r_{\rm O}$/a.u.	t
$BaMoO_3$	0[26]	4.039	–24829.910974	–13.5800	2.86	2.02	1.001
	10	4.008	–24829.913419	–13.5917	2.83	2.00	1.000
	20	3.954	–24829.913851	–13.5976	2.80	1.98	1.000
	30	3.909	–24829.914616	–13.6080	2.76	1.95	1.000
	40	3.871	–24829.915517	–13.6202	2.74	1.94	0.999
	50	3.838	–24829.915843	–13.6247	2.71	1.92	0.999
$SrMoO_3$	0[26]	3.999	–14910.858826	–13.5400	2.83	2.00	1.000
	10	3.945	–14910.861837	–13.6300	2.79	1.97	1.001
	20	3.893	–14910.862262	–13.6358	2.75	1.94	1.002
	30	3.849	–14910.863256	–13.6493	2.72	1.92	1.001
	40	3.811	–14910.863698	–13.6553	2.69	1.90	1.001
	50	3.778	–14910.864152	–13.6615	2.67	1.89	0.999

3.2. Electronic morphology of ZMO's

The calculated total density of states (DOS) and the band structure along the principal symmetry points in the first Brillouin zone are used to predict the electronic morphology of ZMO under variant pressures, the results are plotted in Figs. 2–4. These compounds have metalic and anti-feromagnetic character since the conduction band crosses the Fermi level toward the valence band. The induced pressure has effects on the interatomic distances and on the lattice constants as well which shifts the valence and conduction bands to the higher energies and increases the Fermi energy accordingly. The narrow indirect (M–Γ) band gap that is located around 2.0 eV above the Fermi level for BMO and SMO compounds decreases as the pressure increases. This behavior agrees with the fact that the band-gap of perovskite undergoes a transition from indirect to direct band gap with increased pressure.[8,10,43]

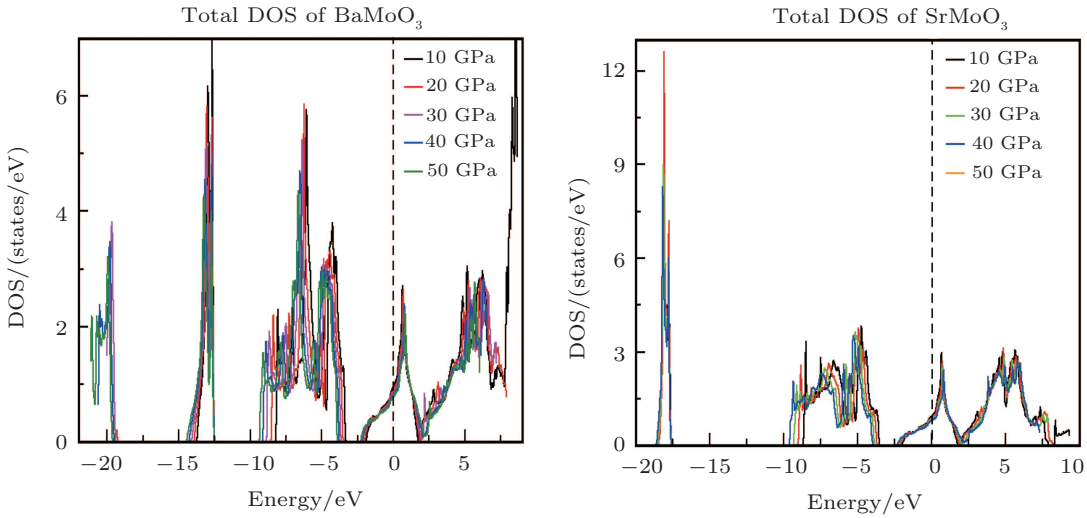


Fig. 2. Total DOS of BMO and SMO under pressure.

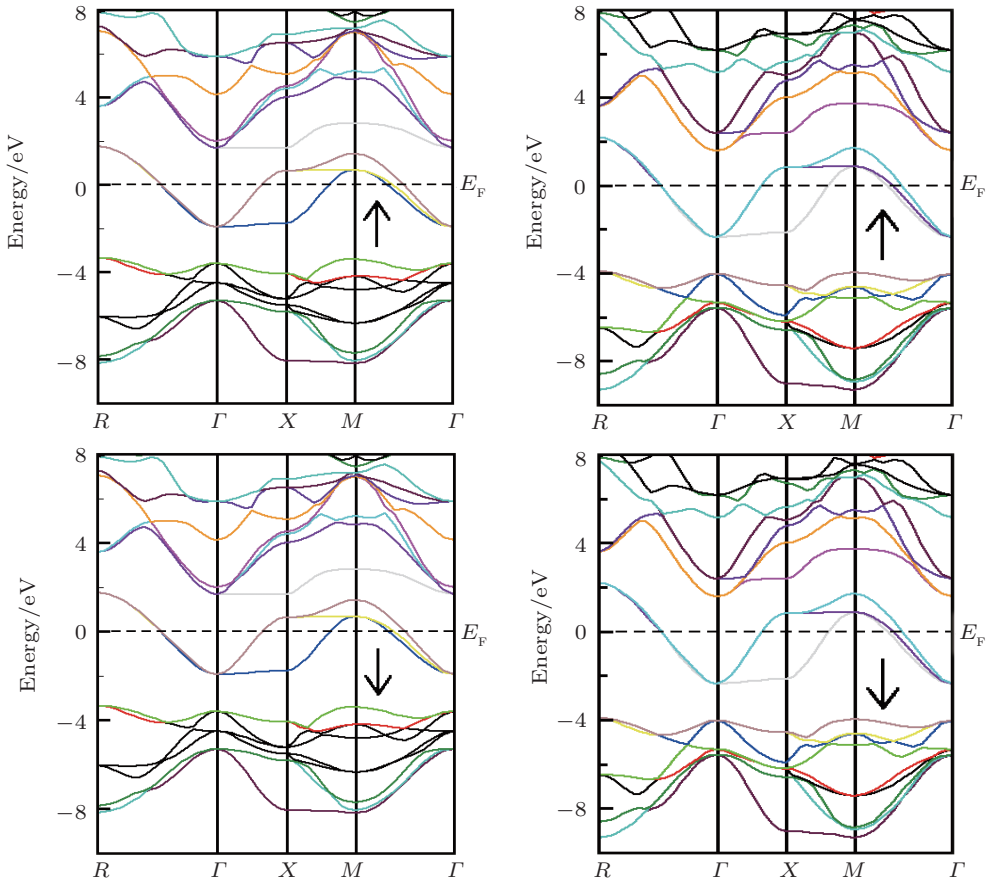


Fig. 3. Electronic band structure of BMO.

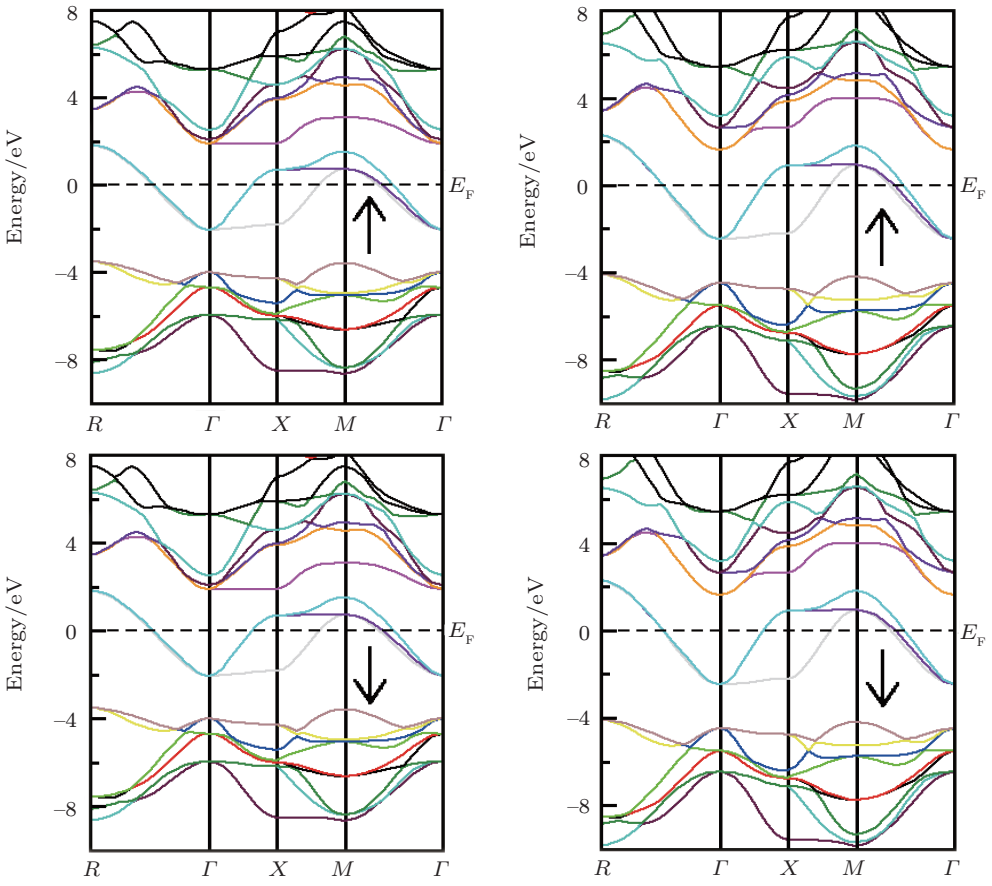


Fig. 4. Electronic band structure of SMO.

3.3. Mechanical attributes of ZMO

Mechanical behavior elucidates how a material withstands stress deformity. Under pressure treatment is quite successful to endure valuable information regarding the cohesion and stiffness of materials. Using numerical first-principle approach embodied in WIEN2k, we have obtained three independent elastic constants C_{ij} (C_{11}, C_{12}, and C_{44}), as listed in Table 2.

Table 2. Pressure P, elastic constants C_{ij}, and elastic anisotropy A.

Compound	P/GPa	C_{11}/GPa	C_{12}/GPa	C_{44}/GPa	A
$BaMoO_3$	0[26]	349.9	120.9	81.6	0.71
	10	404.3	121.4	92.9	0.66
	20	460.6	150.0	114.7	0.74
	30	549.8	158.4	129.7	0.66
	40	637.1	165.4	135.0	0.57
	50	701.9	181.0	158.4	0.61
$SrMoO_3$	0[26]	349.6	108.6	67.7	0.56
	10	434.0	117.7	65.6	0.41
	20	522.2	129.4	86.0	0.44
	30	601.7	143.8	94.0	0.41
	40	659.2	165.7	104.7	0.42
	50	748.6	170.5	111.9	0.39

The stability of the cubic quantum systems can be checked, under stable equilibrium, by satisfying the criterion $(C_{11}-C_{12})>0$, $C_{11}>0$, $C_{44}>0$, and $B>0$.[46] We have found that ZMO sustained stable cubic phase under high pressure by implementing the aforementioned criteria. Elastic anisotropy A delineates the ratio along [100] to [110] direction of shear modulus. The material is assumed to be isotropic for the value of elastic anisotropy being one, whereas, the deviation from this unity assumes the degree of anisotropy for the material. Table 2 predicts that BMO and SMO are anisotropic compounds.

Klienmen parameter ξ, presented in Table 3, interprets ease of minimizing bond bending, bond stretching, and it is directly related to piezoelectricity. For $\xi \to 0$, in bond bending minimization, piezoelectricity decreases, whereas for $\xi \to 1$, in bond stretching situation, piezoelectricity increases. For BMO, we have found that ξ decreases as induced pressure increases, with exception at 20 GPa. This phenomenon can be explained with the help of anisotropy parameter listed in Table 2. We have found that for BMO, the observed anisotropy at 20 GPa is maximum, *i.e.*, 0.74 which indicates a large directional dependent property of the compound. Thus, piezoelectric or internal strain parameter ξ indicates the different response at 20 GPa as compared to the other computed values. While for SMO, the abrupt increase in the value of ξ is because of near about transition from indirect to direct band gap at 40 GPa and above.

ZMO compounds exhibit ductile nature according to Pough's (B/G) and Frantsevich's (G/B) ratios. Ductile nature can be estimated by $(B/G)>1.75$ and $(G/B)<0.57$ and brittle nature of compound by $(B/G)<1.75$ and $(G/B)>0.571$. All the mentioned properties can be observed with the help of Table 3.

Tetragonal shear constant $C_\alpha = 0.5(C_{11}-C_{12})$ explains the dynamical stability. For $C_\alpha > 0$, material is stable, and $C_\alpha < 0$ portrays an unstable structure. For $C_\alpha \to 0$, the material exhibits superplastic deformation. In the present study, ZMO does not exhibit plastic deformation[47] which is obtained by

$$\delta = \frac{(6C_{44})(C_{11}-C_{12})}{(C_{11}-C_{12})+8C_{44}}.$$

We have also appraised the hardness of ZMO's using Vickers hardness H_V:[48] $H_V = 0.92(G/B)^{1.137}G^{0.708}$. This property expounds the capability of ZMO's to confront against being dented. We have found in our study that hardness of BMO is higher than SMO under all the pressure range. Moreover, the induced pressure increases the hardness of the stable present compounds by decreasing the interatomic distances between the content atoms.

Table 3. Pressure P, bulk modulus B, shear modulus G, Young modulus E, hardness H_a, super plasticity , melting temperature T_M, Debye temperature Θ, minimum thermal conductivity Λ_{min} (at 0 K), Kleinman parameter ξ, and Gruninsen parameter γ.

Compound	P/GPa	B/GPa	G/GPa	E/GPa	H_aGPa	δ/GPa	T_M/K±300	Θ/K	Λ_{min}/W·K^{-1}·m^{-1}	ξ	γ
$BaMoO_3$	0[26]	197	93	242	–	–	2620.87	391.14	–	0.490	–
	10	216	110	282	0.028	0.154	2942.59	421.92	0.6728	0.448	3.334
	20	254	130	332	0.032	0.174	3275.02	454.73	0.7349	0.471	3.330
	30	289	153	390	0.037	0.213	3802.27	491.07	0.7992	0.436	3.254
	40	323	169	432	0.039	0.246	4318.11	513.86	0.8456	0.409	3.276
	50	355	194	491	0.045	0.279	4701.20	546.83	0.9034	0.408	3.192
$SrMoO_3$	0[26]	189	85	223	–	–	2619.12	410.54	–	0.460	–
	10	223	94	248	0.020	0.148	3117.86	428.60	0.7112	0.420	3.740
	20	260	121	313	0.027	0.188	3639.28	480.82	0.7988	0.398	3.538
	30	296	136	353	0.029	0.213	4108.97	507.03	0.8534	0.389	3.566
	40	330	149	388	0.030	0.233	4449.05	528.73	0.9005	0.401	3.598
	50	363	166	431	0.033	0.263	4976.94	555.15	0.9523	0.378	3.573

We have calculated the Cauchy pressure, $C'' = C_{12} - C_{44}$, which is used to analyze the origin of angular attributes of atomic bonding present in the unit cell. For a negative value of C'', the majority of the bonds of a compound exhibits covalent bonding. While, for a positive value of C'', ionic bonding is retained in majority of the bonds. Johnson[49] and Pettifor[50] suggested the positive values of C'' as a metallic character. In our study, ZMO's exhibit majority of the bonds in the unit cell as having ionic character along with a metallic nature of the compounds. The increase in the measured value of C'' under pressure suggests a more metallic nature.

We have calculated Debye temperature Θ[51] and the melting temperature T_M[52] from the relations

$$\Theta = \left[\frac{h}{k}\right]\left[\frac{3n}{4\pi}\left(\frac{N_A\rho}{M}\right)\right]^{1/3} V_m$$

and $T_M = 553 + (5.91 \times C_{11})$/GPa, respectively, where v_l and v_t, the longitudinal and transverse wave velocities, respectively, are used to calculate V_m, *i.e.*, average sound velocity[53]

$$V_m = \left[\frac{1}{3}\left(\frac{2}{v_t^3} + \frac{1}{v_l^3}\right)\right]^{-1/3}.$$

For the temperature range $\Theta < T < T_M$, the high-frequency mode of phonon oscillations may occur. For $T < \Theta$, phonon oscillations would expect to be frozen. The increase in Debye and melting temperatures agrees with the hardness results that are found above with the increasing pressure. The calculated Debye and melting temperature values show the high modes of oscillations in BMO and SMO under variant pressure. This characteristic of BMO and SMO may have applications in the appliances which work at high temperatures.

Gruninsen parameter γ may also suggest a degree of anharmonicity in the chemical bond. The higher the Gruninsen value, the higher the anharmonicity, which generally drives greater phonon-phonon scattering. We have calculated the Gruninsen parameter using relation[54] $\gamma = [3(1+\mu)]/[2(2-3\mu)]$.

In the case of BMO, we have found that γ decreases as the pressure increases up to 30 GPa and then suddenly the calculated value of γ increases at 40 GPa and then decreases again as the pressure increases at 50 GPa. Whereas, the calculated value of γ for SMO decreases with the increase of pressure up to 20 GPa then suddenly increases at 40 GPa and then returns to a decrease at 50-GPa pressure. We conclude from Table 3 that this abrupt behavior for both SMO and BMO is because of shifting in electronic states from indirect to nearly direct band gap transition. This is because of electronic configuration of Ba and Sr atoms. For Ba atom the ionic radius (268 pm) and filled electronic states ($1s^2$, $2s^2$, $2p^6$, $3s^2$, $3p^6$, $3d^{10}$, $4s^2$, $4p^6$, $4d^{10}5s^2$, $5p^6$, and $6s^2$) are higher than Sr with an ionic radius of 255 pm and filled electronic states ($1s^2$, $2s^2$, $2p^6$, $3s^2$, $3p^6$, $3d^{10}$, $4s^2$, $4p^6$, and $5s^2$). Once the states become available with minimum energy to form a stable chemical bond for conduction, it increases the anharmonicity with the increase of pressure. After the occurrence of transition and stability, it decreases. The available conduction states in case of Sr begin to transform from indirect to direct at 30 GPa, prior to Ba where it occurs at 40 GPa. The full transition from indirect to direct band gap occurs above 50 GPa for both the compounds. Using Cahill criteria,[55] minimum thermal conductivity Λ_{min} of BMO and SMO have been computed from $\Lambda_{min} = (k/2.48)(n_b)^{2/3}(V_L + 2V_T)$, where n_b, k, V_T, and V_L are number of atoms per unit volume, Boltzmann constant, transversal and longitudinal sound velocities, respectively.

To the best of the author's knowledge, there is no data (experimental or theoretical) available in literature for the comparison of the elastic and thermal properties of these compounds under pressure. So, our results can be used for comparison in future experimental or theoretical investigations.

3.4. Optical treatment of ZMO under pressure

The complex dielectric function, $\varepsilon(\omega) = \varepsilon_1(\omega) + i\varepsilon_2(\omega)$, is used to depict the response of the applied electromagnetic field and to calculate the optical properties of the $BaMoO_3$ and $SrMoO_3$ compounds. The imaginary $\varepsilon_2(\omega)$ and real $\varepsilon_1(\omega)$, part of the dielectric function for the $BaMoO_3$ and $SrMoO_3$ compounds, are calculated for different values of pressure in the energy range up to 35.0 eV, as shown in Figs. 5 and 6, respectively.

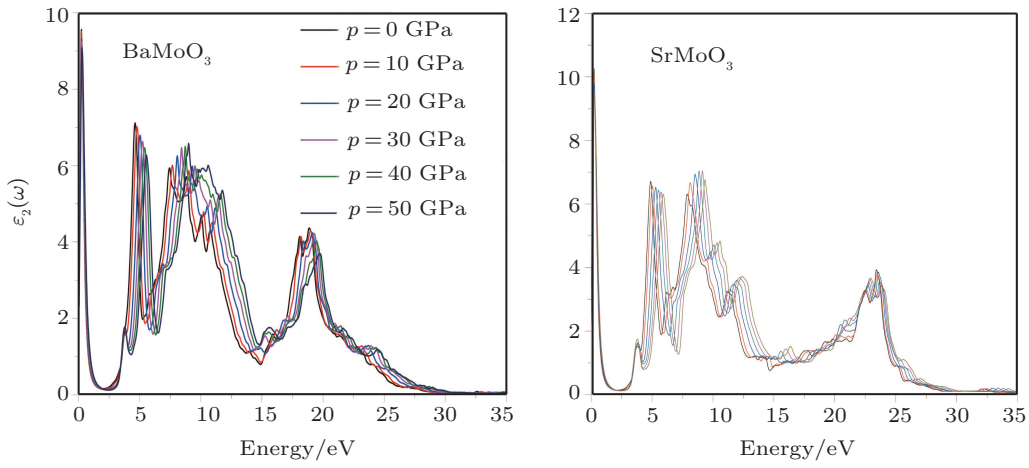


Fig. 5. The imaginary part $\varepsilon_2(\omega)$ of the dielectric function $\varepsilon(\omega)$ for BMO and SMO.

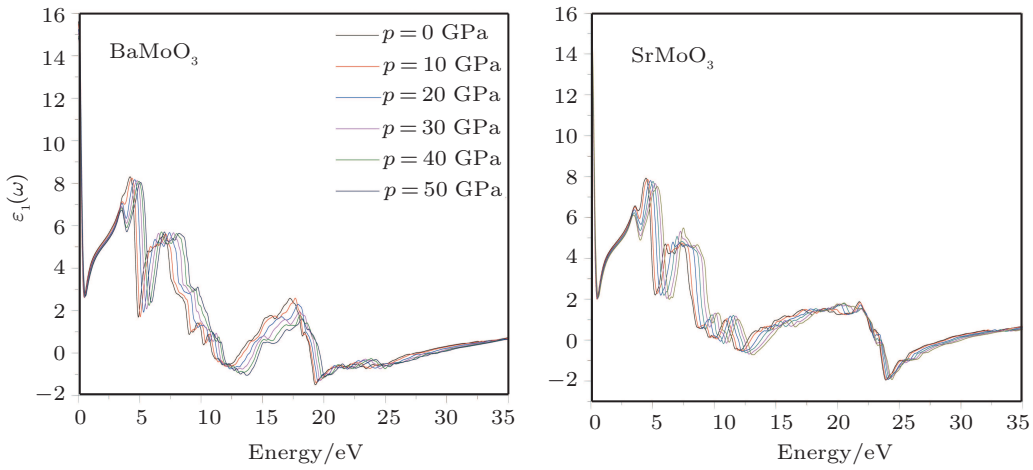


Fig. 6. The real part $\varepsilon_1(\omega)$ of the dielectric function $\varepsilon(\omega)$ for BMO and SMO.

The $\varepsilon_2(\omega)$ spectrum is calculated by considering all possible transitions from the valence to the conduction states that are calculated by the following matrix formula:[56]

$$\varepsilon_2(\omega) = \left(\frac{\hbar^2 e^2}{\pi m^2 \omega^2}\right) \sum_{c,v} \int \mathrm{d}^3 k \langle c_k | p^\alpha | v_k \rangle \langle v_k | p^\beta | c_k \rangle \delta(\varepsilon_{ck} - \varepsilon_{vk} - \omega), \tag{1}$$

where p is the momentum matrix element between α and β bands states with momentum k, v_k, and c_k are the crystal wave functions corresponding to the valence and conduction bands with crystal wave vector.

The zero-frequency limit of the calculated $\varepsilon_2(0)$ of the BMO and SMO compounds are found to be 3.14 and 2.26 for the variant pressure, respectively. These values appear as a result of crossing the valence bands of Mo-d and O-p states to the conduction bands through Fermi level. Beyond these points, the different spectra have increased sharply and reached the maximum sharp peak around 9.56 for BMO and 10.27 for SMO. The spectra have decreased sharply and reached zero approximately. The threshold point energy of $\varepsilon_2(\omega)$ is represented by the fundamental absorption edges. These points occur around 2.68 eV and 2.93 eV for the variant pressure of the BMO and SMO compounds, respectively, which are due to the electrons transitioning from Mo-d and O-p states of the valence bands to Mo-d and O-p states of conduction bands. The effect of the pressure on the calculated fundamental absorption edges values is not observed because the locations of the valence and conduction bands around Fermi level are approximately the same. The spectra are increased as a result of the increase in the number of points that are participating toward $\varepsilon_2(\omega)$. The first peaks are located around 3.82 eV and 3.80 eV for the variant applied pressure of the BMO and SMO compounds, respectively. These are due to the transitions of electrons from the Mo-d and O-p states of the valence band to the Mo-d and O-p states of the unoccupied conduction bands. Beyond the first peak, the spectra are found to be distinguishable and have the same character for different applied pressures. This dispersion is due to the small difference in the locations of the valence and conduction bands. The $\varepsilon_2(\omega)$ spectra are fluctuated to reach a saturation. The second peak is related to the contribution of the electron transition from the occupied Mo-d and O-p states of the valence band to the Mo-d, Ba-d (or Sr-d), and O-p states of the unoccupied conduction bands.

The $\varepsilon_1(\omega)$ spectra of the BMO and SMO compounds are calculated from $\varepsilon_2(\omega)$ using Kramers–Kronig dispersion relation[56]

$$\varepsilon_1(\omega) = 1 + \frac{2}{\pi} P \int_0^\infty \frac{\omega' \varepsilon_2(\omega') \mathrm{d}\omega'}{(\omega'^2 - \omega^2)}, \tag{2}$$

where P represents the principal value of the integral.

The zero frequency limits of the real part of the dielectric function, $\varepsilon_1(0)$, represents the static dielectric constant. The calculated $\varepsilon_1(0)$ values are found around 15.62 and 15.76 for the BMO and SMO compounds, respectively. These values are found higher than that calculated for the $BaTiO_3$ and $SrTiO_3$ compounds[57] since the present compounds have a metallic character. The effect of the applied pressure on the $\varepsilon_1(\omega)$ values appears above 3.50 eV approximately. The $\varepsilon_1(\omega)$ spectra reach the maximum value at 0 GPa, of 8.30 around 4.23 eV for BMO and 7.92 around 4.48 eV for SMO. The maximum values of $\varepsilon_1(\omega)$ are found to be decreasing as the applied pressure increases. The spectra are fluctuated to reach the negative values in the different energy ranges. In these ranges, the compounds are assumed to have a metallic character. Both compounds have a high dielectric constant which can be assumed to have useful microelectronic industrial applications.

The optical spectra such as the refractive index $n(\omega)$, reflectivity $R(\omega)$, absorption coefficient $I(\omega)$, energy loss function $L(\omega)$, and optical conductivity $\sigma(\omega)$, are computed in terms of $\varepsilon_1(\omega)$ and $\varepsilon_2(\omega)$ with the following formulas:[56]

$$n(\omega) = \left[\frac{\sqrt{\varepsilon_1^2(\omega)+\varepsilon_2^2(\omega)}+\varepsilon_1(\omega)}{2}\right]^{1/2}, \tag{3a}$$

$$R(\omega) = \frac{n+\mathrm{i}k-1}{n+\mathrm{i}k+1}, \tag{3b}$$

$$I(\omega) = 2\omega k(\omega), \tag{3c}$$

$$L(\omega) = \frac{\varepsilon_2(\omega)}{\varepsilon_1^2(\omega)+\varepsilon_2^2(\omega)}, \tag{3d}$$

$$\varepsilon(\omega) = \varepsilon_0(\omega)+\frac{4\pi\mathrm{i}\sigma(\omega)}{\omega}. \tag{3e}$$

The calculated refractive index spectra of BMO and SMO are shown in Fig. 7, respectively. The zero-frequency limit of the refractive index, $n(0)$, represents the static refractive index which is an important optical parameter. This calculated parameter is found about 3.97 and 4.00 for BMO and SMO, respectively. These values are approximately equal for both of the present compounds under the variant applied pressure because the conduction bands of the present compounds have the same character. The $n(0)$ values of the present compounds are found higher than that computed for $BaTiO_3$ and $SrTiO_3$.[57] This variation is due to the metallic behavior of the present compounds around Fermi level. The $n(\omega)$ spectra decrease sharply then they are fluctuating. In the high energy level, the computed $n(\omega)$ value is less than unity and reaches its minimum value at about 0.23 for both the compounds. In this region, the present compounds are expected to be superluminal for high energy photons.

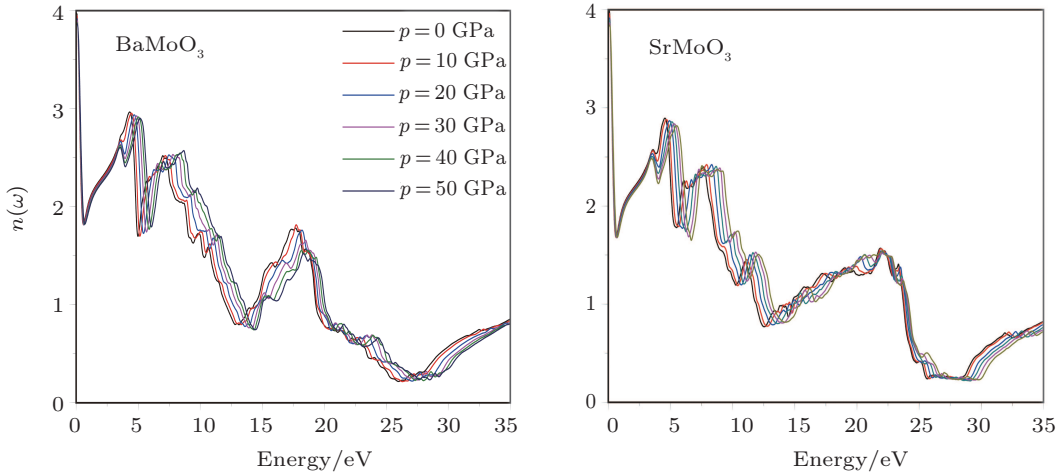


Fig. 7. The refractive index $n(\omega)$ of the dielectric function $\varepsilon(\omega)$ for BMO and SMO.

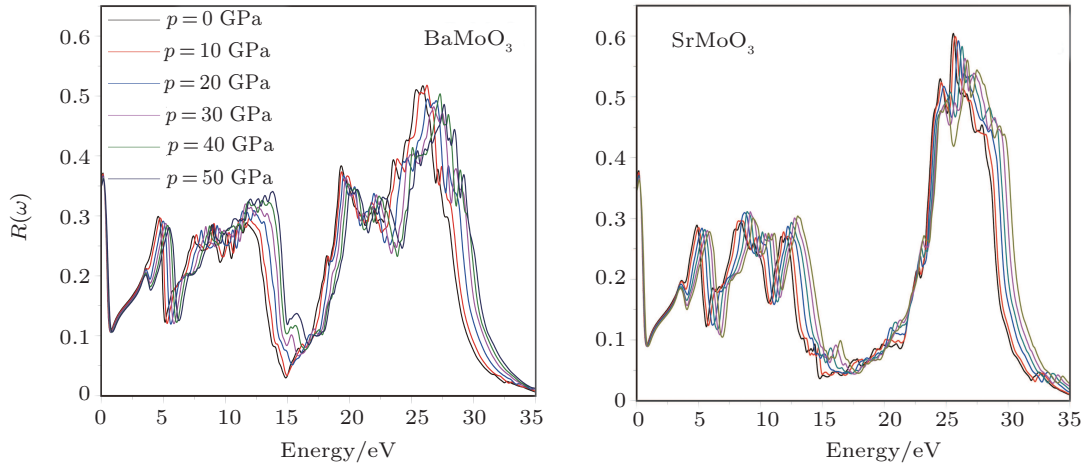


Fig. 8. The reflectivity $R(\omega)$ of the dielectric function $\varepsilon(\omega)$ for BMO and SMO.

Figure 8 presents the calculated reflectivity spectra of the studied compounds. The zero-frequency limit of $R(0)$ for the BMO and SMO compounds under the variant applied pressure is found at 36.1% and 36.3%, respectively. Beyond $R(0)$ value, the $R(\omega)$ spectra decrease sharply then fluctuate to reach minimum value under 0 GPa about 3.0% at 14.87 eV and 3.6% at 14.82 eV for the BMO and SMO compounds, respectively. The maximum calculated $R(\omega)$ value is found around

51.7% at 25.92 eV and 60.4% at 25.59 eV under 0 GPa for the BMO and SMO compounds, respectively. The calculated $R(\omega)$ is found to be higher than 10% in the most part of the energy range. From this behavior, we can expect that the present compounds have a high ability in avoiding a solar heating and beneficial for the thermoelectric applications. In the energy range 13.67 eV–16.85 eV for BMO and 13.35 eV–25.59 eV for SMO, the $R(\omega)$ values are lower than 10% and the incident photons have a high transparency through the compounds. Thus, we can expect that in this energy region, the present compounds under the variant pressure could be used as anti-reflection coating and lenses. The minimum and maximum calculated $R(\omega)$ values of the present compounds are slightly varying under applied pressure due to minute distinctions that occur in their conduction band. These variations shift the $R(\omega)$ curve to the high energy level that yields to increase the solar sheltering heating in the energy around 15.0 eV due to the increase of the pressure. At the energy around 26.0 eV, the $R(\omega)$ value is slightly decreased due to pressure. We suggest that for the present compounds, the values of reflectivity differ slightly, depending on the energy level with small effect from the applied pressure.

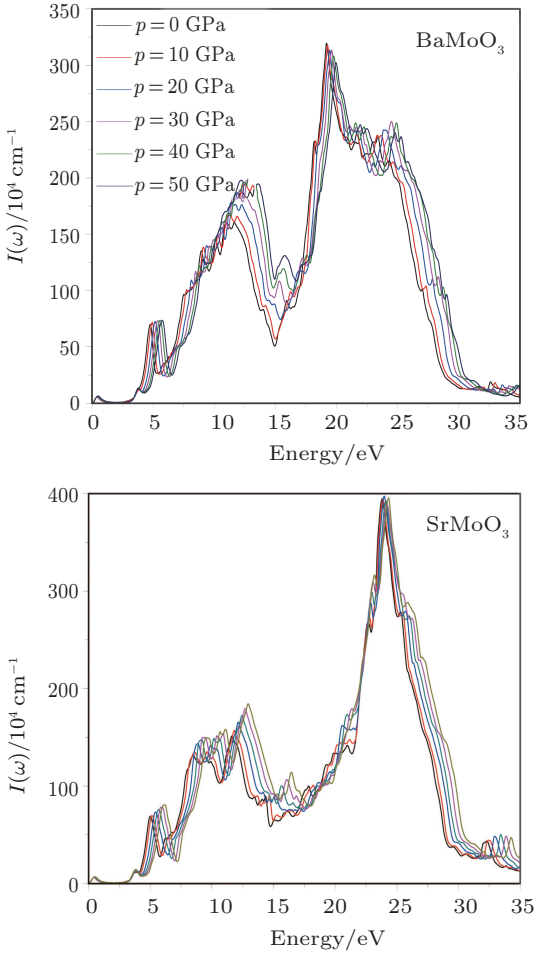


Fig. 9. The absorption coefficient $I(\omega)$ of the dielectric function $\varepsilon(\omega)$ for BMO and SMO.

The calculated absorption coefficient $I(\omega)$ of the present compounds as a function of energy are displayed in Fig. 9. The effective energy point from which a compound starts absorbing the electromagnetic radiations sharply is called the threshold in $I(\omega)$. This energy is found around 2.92 eV and 3.09 eV for BMO and SMO, respectively. In the high energy level, the maximum $I(\omega)$ value is found to be 318.5×10^4 cm^{-1} at 19.22 eV for BMO and 394.5×10^4 cm^{-1} at 23.82 eV for SMO under 0 GPa. These values are found lower than that calculated for $BaTiO_3$ and $SrTiO_3$.[57] Both compounds have a high absorption coefficient in the ultraviolet spectrum region.

The electron energy loss function $L(\omega)$ depicts the plasmon oscillations of the electrons passing through the compound that is shown in Fig. 10. The plasmon peak is the sharpest resonant peak that appears in $L(\omega)$ spectrum. These peaks are found at around 25.37 eV and 28.69 eV for BMO and SMO under 0 GPa, respectively. The plasmon peak traverses to the high energy level as the applied pressure on the compound increases. At these peaks, the calculated $\varepsilon_1(\omega)$ value approaches zero.

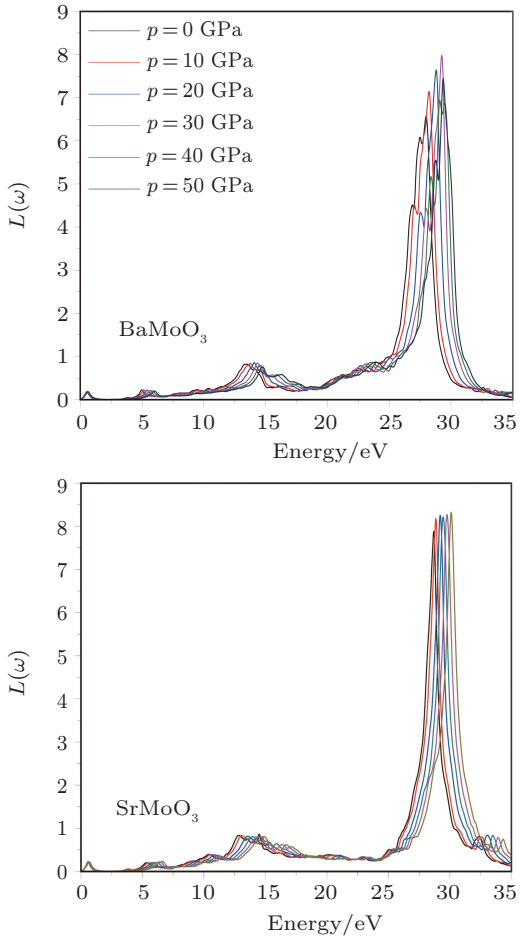


Fig. 10. The electron energy loss function $L(\omega)$ of the dielectric function $\varepsilon(\omega)$ for BMO and SMO.

Figure 11 presents the optical conductivity $\sigma(\omega)$ spectra of the studied compounds. These spectra depict the conduction of the electrons due to the applied electromagnetic field.

The threshold points in $\sigma(\omega)$ are located around 2.92 eV and 3.09 eV for BMO and SMO, respectively. These points are consistent with the calculated threshold points in $I(\omega)$. The calculated highest peak of $\sigma(\omega)$ is around 11082 $\Omega^{-1}\cdot\text{cm}^{-1}$ around 18.87 eV for BMO and 12395 $\Omega^{-1}\cdot\text{cm}^{-1}$ at 23.41 eV for SMO. At these extrema points, the $\varepsilon_1(\omega)$ spectrum is in the negative region and the studied compounds have metallic behavior. The calculated maximum peak value of the studied compound is found to be lower than that calculated for $SrTiO_3$ and $BaTiO_3$.[57] We expect that BMO and SMO compounds are more effective protecting material from solar heating than $SrTiO_3$ and $BaTiO_3$ due to their high optical parameters.

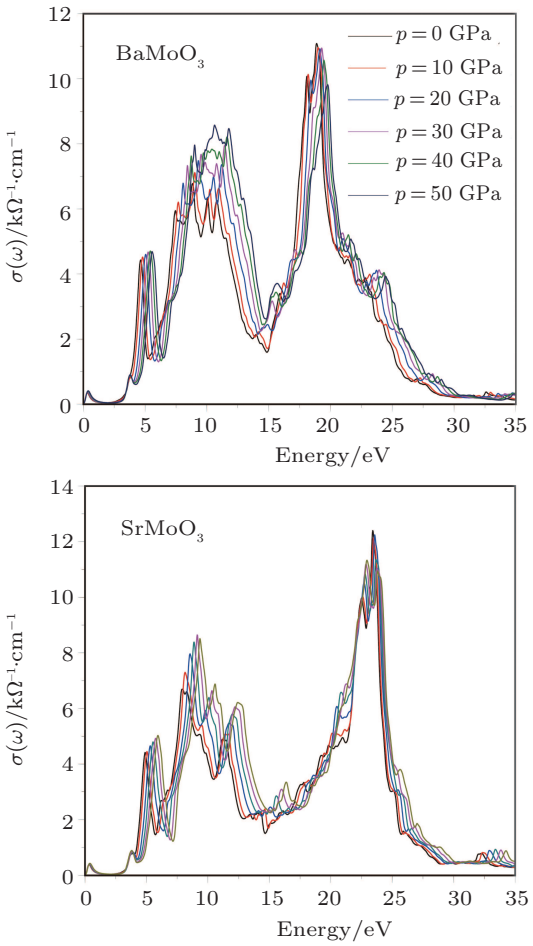


Fig. 11. The optical conductivity $\sigma(\omega)$ of the dielectric function $\varepsilon(\omega)$ for BMO and SMO.

The oscillator strength of the sum rule spectra $N(\omega)$ for the present compounds is displayed in Fig. 12. These spectra are used to calculate the effective number of valence electrons per unit cell that are contributing in the inter-band transitions. The calculated effective number of electrons is zero up to 3.54 eV. Beyond that, the $N(\omega)$ spectra are increased until they saturate at about 26.46 eV for BMO and 28.45 eV for SMO. This shows that the deep lying valence states do not participate in the inter-band transition.

The optical results expect that the BMO and SMO compounds own beneficial optical applications in high energy regions due to their high optical conductivity and absorption range. It is found that there are no significant variations in the calculated optical spectra of the present compounds under the variant applied pressure due to their conduction bands being almost the same.

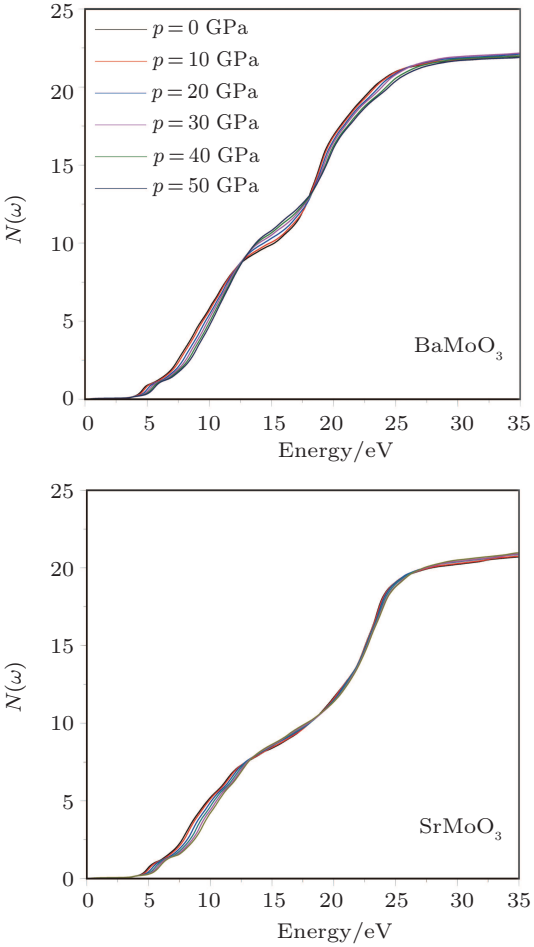


Fig. 12. The sum rule $N(\omega)$ of the dielectric function $\varepsilon(\omega)$ for BMO and SMO.

4. Conclusions

First principles calculations based on density functional theory (DFT) are used to perform the structural, electronic, elastic, and optical properties of the cubic $ZMoO_3$ (Z = Ba and Sr) molybdates in the pressure range of 10 GPa–50 GPa. The enthalpy of formation energy and elastic constants predict that the present compounds are thermodynamically and elastically stable under pressure up to 50 GPa. The electronic properties predict that BMO and SMO have anti-ferromagnetic and metallic characters. These compounds exhibit anisotropic, ductile, and ionic bond nature. The hardness and metallic nature of BMO are found to be higher than that expected for SMO. These nature properties are predicting to increase as pressure is increasing. BMO and SMO expect to own beneficial industrial applications for appliances that work at high temperature under variant pressure. The optical properties of BMO and SMO are investigated using the real and imaginary

part of dielectric function. The main peaks in the optical spectra are discussed using the projected density of states for the content atoms. The static refractive indices of BMO and SMO are found to be about 3.97 and 4.00. The optical parameter values have small variation under the variant applied pressure. The different optical parameters of BMO are found higher than that computed for SMO. Due to the optical properties of BMO and SMO, we predict these compounds are useful in the anti-reflection coating, lenses, and the high avoiding solar heating applications in the variant applied pressure.

Acknowledgement

We are thankful to Dr. Afaq Ahmad for his useful discussions in completing this work.

References

[1] Lu Y, Lu W G and Wang L 2017 *Chin. Phys. Lett.* **34** 017102
[2] Sun J H and Tang H K 2018 *Chin. Phys. B* **27** 077502
[3] Li X Y, Huang C, Zhu Y, Li J B, Fan J Y, Pan Y F, Shi D N and Ma C L 2018 *Acta Phys. Sin.* **67** 137101 (in Chinese)
[4] Xiao H Y, Qin Y K, Liu L N, *et al.*2018 *Acta Phys. Sin.* **67** 140702 (in Chinese)
[5] Meng K K, Zhao X P, Miao J, Xu X H, Zhao J H and Jiang Y 2018 *Acta Phys. Sin.* **67** 131202 (in Chinese)
[6] Jiang Y Q and Peng P 2018 *Acta Phys. Sin.* **67** 132101 (in Chinese)
[7] Huang L, Liu W L and Deng C S 2018 *Acta Phys. Sin.* **67** 136101 (in Chinese)
[8] Tariq S, *et al.* 2015 *AIP Adv.* **5** 077111
[9] Nadeem S *et al.* 2016 *J. Theor. Comput. Chem.* **15** 1650044
[10] Nazi G, *et al.* 2015 *Comput. Condens. Matter* **4** 32
[11] Gilani S S, *et al.* 2018 *Chin. J. Phys.* **56** 308
[12] Jin F, *et al.* 2018 *Chin. Phys. B* **27** 077801
[13] Deligoz E, Ozisik H and Colakoglu K 2014 *Philos. Mag.* **94** 1379
[14] Ozisik H B, Ozisik H and Deligoz E 2017 *Philos. Mag.* **97** 549
[15] Korozlu N, Colakoglu K and Deligoz E 2009 *J. Phys.: Condens. Matter* **21** 175406
[16] Scott J 2007 *Science* **315** 954
[17] Cross E 2004 *Nature* **432** 24
[18] Schneider T, et al. 2007 *Opt. Mater.* **29** 1871
[19] Watton R 1989 *Ferroelectrics* **91** 87
[20] Liu P, *et al.* 2017 *Chin Phys Lett.* **34** 027101
[21] Zhao Q Z and Zhang D L 2017 *Chin Phys Lett.* **34** 034207
[22] Li Z and Zheng G Q 2018 *Chin. Phys. B* **27** 077404
[23] Sun J P and Zhang D 2017 *Chin. Phys. Lett.* **34** 027102
[24] Zhu P, *et al.* 2018 *Chin. Phys. B* **27** 076103
[25] Cheng J G, *et al.* 2018 *Chin. Phys. B* **27** 077403
[26] Tariq S, *et al.*2018 *Appl Phys A* **124** 44
[27] Nassif V, Carbonio R E and Alonso J A 1999 *J. Solid State Chem.* **146** 266
[28] Mizoguchi H, *et al.* 1999 *J. Appl. Phys.* **85** 6502
[29] Mizoguchi H, *et al.* 2000 *J. Appl. Phys.* **87** 4617
[30] Kurosaki K, *et al.* 2004 *J. Alloys Compd.* **372** 65
[31] Kubo J and Ueda W 2009 *Mater. Res. Bull.* **44** 906
[32] Wang H, *et al.* 2001 *J. Cryst. Growth* **226** 261
[33] Radetinac A, *et al.* 2014 *Appl. Phys. Lett.* **105** 114108
[34] Sahu M, *et al.* 2015 *J. Nucl. Mater.* **457** 29
[35] Hopper H, *et al.* 2016 *J. Solid State Chem.* **234** 87
[36] Brixner L 1960 *J. Inorg. Nucl. Chem.* **14** 225
[37] Scholder R and Klemm W 1954 *Angewandte Chemie* **66** 461
[38] Andersen O K 1975 *Phys. Rev. B* **12** 3060
[39] Perdew J P, *et al.* 1992 *Phys. Rev. B* **46** 6671
[40] Singh D J and Nordstrom L 2006 *Planewaves, Pseudopotentials, and the LAPW Method* (Springer Science & Business Media)
[41] Blaha P, *et al.* 2001 *wien2k, An augmented plane wave+ local orbitals program for calculating crystal properties*, ISBN 3-9501031-1-2
[42] Perdew J P, Burke K and Ernzerhof M 1996 *Phys. Rev. Lett.* **77** 3865
[43] Nazir G, *et al.* 2018 *Acta Phys. Polon. Ser. A* **133** 105
[44] Murnaghan F D 1944 *Proc. Natl. Acad. Sci. USA* **30** 244
[45] Goldschmidt V M 1926 *Naturwissenschaften* **14** 477
[46] Karki B, Ackland G and Crain J 1997 *J. Phys.: Condens. Matter* **9** 8579
[47] Souvatzis P, et al. 2004 *Phys. Rev. B* **70** 012201
[48] Tian Y, Xu B and Zhao Z 2012 *J. Refract. Met. Hard Mater.* **33** 93
[49] Johnson R 1988 *Phys. Rev. B* **37** 3924
[50] Pettifor D 1992 *Mater. Sci. Technol.* **8** 345
[51] Hao Y J, *et al.* 2006 *Physica B* **382** 118
[52] Fine M, Brown L and Marcus H 1984 *Scr. Metall.* **18** 951
[53] Screiber E, Anderson O and Soga N 1973 *Elastic Constants and Their Measurements* (New York: McGrawHill), ISBN-10: 0070556032, ISBN-13: 978-0070556034
[54] Blanco M, Francisco E and Luana V 2004 *Comput. Phys. Commun.* **158** 57
[55] Cahill D G, Watson S K and Pohl R O 1992 *Phys. Rev.* **46** 6131
[56] Fox M 2002 *Optical Properties of Solids* (Oxford: Oxford University Press) pp. 2–7, ISBN 978-0-19-850613-3
[57] Mubarak A A 2016 *Int. J. Mod. Phys B* **30** 1650141